Architectural analysis on dynamic MRI to study thoracic insufficiency syndrome

Jie Song, Jayaram K. Udupa, Yubing Tong, Liang Xiao, Caiyun Wu, et al.

Jie Song, Jayaram K. Udupa, Yubing Tong, Liang Xiao, Caiyun Wu, Joseph McDonough, Anthony Capraro, Drew A. Torigian, Robert M. Campbell, "Architectural analysis on dynamic MRI to study thoracic insufficiency syndrome," Proc. SPIE 10576, Medical Imaging 2018: Image-Guided Procedures, Robotic Interventions, and Modeling, 105762C (13 March 2018); doi: 10.1117/12.2294551

SPIE.

Event: SPIE Medical Imaging, 2018, Houston, Texas, United States

Architectural Analysis on Dynamic MRI to Study Thoracic Insufficiency Syndrome

Jie Song[1, 3], Jayaram K. Udupa[1], Yubing Tong[1], Liang Xiao[3], Caiyun Wu[1], Joseph McDonough[2], Anthony Capraro[2], Drew A. Torigian[1], Robert M. Campbell Jr.[2]

[1]Medical Image Processing Group, 602 Goddard building, 3710 Hamilton Walk, Department of Radiology, University of Pennsylvania, Philadelphia, PA 19104

[2]Center for Thoracic Insufficiency Syndrome, Children's Hospital of Philadelphia, Philadelphia, PA, 19104

[3]Department of Computer Science and Technology, Nanjing University of Science and Technology, Nanjing, 210094

ABSTRACT

The major hurdles currently preventing advance and innovation in thoracic insufficiency syndrome (TIS) assessment and treatment are the lack of standardizable objective diagnostic measurement techniques that describe the 3D thoraco-abdominal structures and the dynamics of respiration. Our goal is to develop, test, and evaluate a quantitative dynamic magnetic resonance imaging (QdMRI) methodology and a biomechanical understanding for deriving key quantitative parameters from free-tidal-breathing dMRI image data for describing the 3D structure and dynamics of the thoraco-abdominal organs of TIS patients. In this paper, we propose an idea of a shape sketch to codify and then quantify the overall thoracic architecture, which involves the selection of 3D landmark points and computation of 3D dynamic distances over a respiratory cycle. We perform two statistical analyses of distance sketches on 25 different TIS patients to try to understand the pathophysiological mechanisms in relation to spine deformity and to quantitatively evaluate improvements from pre-operative to post-operative states. This QdMRI methodology involves developing: (1) a 4D image construction method; (2) an algorithm for the 4D segmentation of thoraco-abdominal structures; and (3) a set of key quantitative parameters. We illustrate that the TIS dynamic distance analysis method produces results previously unknown and precisely describes the morphologic and dynamic alterations of the thorax in TIS. A set of 3D thoraco-abdominal distances and/or distance differences enables the precise estimation of key measures such as left & right differences, differences over tidal breathing, and differences from pre- to post-operative condition.

Keywords: Thoracic insufficiency syndrome, dynamic magnetic resonance imaging, dynamic distance analysis

1. INTRODUCTION

Extensive thoracic congenital scoliosis associated with fused ribs may affect thoracic function and growth and have an adverse effect on the function and growth of the lungs. This condition is referred to as thoracic insufficiency syndrome (TIS) [1], which is defined as the inability of the thorax to support normal respiration or lung growth. Progressive TIS due to three-dimensional thoracic deformity and dysfunction can be characterized on the basis of the history of respiratory symptoms and the findings on physical examination, radiographs, computed tomography (CT) scans, pulmonary function test studies, and other laboratory tests of respiratory function. Treatment should restore thoracic volume and function and maintain these gains during growth. Outcome assessment of thoracic and spinal surgery for TIS is currently limited to static radiographs. CT scans are not practical because of radiation dose concerns. A relatively new technique, dynamic magnetic resonance imaging (dMRI), has great potential to clearly define quantitatively, without radiation concerns, the dynamic biomechanical deficits and response to treatment of the dynamic thoraco-abdominal organs of young patients with TIS.

Medical Imaging 2018: Image-Guided Procedures, Robotic Interventions, and Modeling, edited by Baowei Fei, Robert J. Webster III, Proc. of SPIE Vol. 10576, 105762C · © 2018 SPIE
CCC code: 1605-7422/18/$18 · doi: 10.1117/12.2294551

Updated 3/20/14

Several studies have shown that different lung functions have little relation to the Cobb angle alone in children with TIS [2, 3]. Given the combinations of structural abnormalities of the vertebrae and ribs producing TIS, and the variations in severity of each structural deformity, it is not surprising that combinations of thoracic and spine structural features, in general, do not correlate well with respiratory functional abnormalities. An alternative approach is to use both the structural and functional measures in conjunction with one another to determine severity and, when used serially, to assess the rate of progression of TIS in young children.

We have been developing a quantitative dMRI (QdMRI) methodology for deriving key quantitative parameters from free-tidal-breathing thoracic dMRI image data for describing the 3D structure and dynamics of the thoraco-abdominal organs of TIS patients. Previously, we proposed methods to compute tidal volumes (change in volumes from end-expiration to end-inspiration) for left and right lungs, chest walls, and hemi-diaphragms from dMRI data sets and showed how to assess post-surgical changes in lung function [4]. Continuing in this direction, in this paper, we investigate how the dynamics of the architecture defined by landmarks identified on these thoracic structures can be analyzed to gain insight into TIS and its treatment.

The main contributions are as follows:

1) General surgeons, orthopedists, and pulmonologists individually treat patients with TIS, but dynamic metrics to measure the severity of TIS and the effectiveness of therapeutic interventions are non-existent. This paper presents a new dynamic analysis technique based on distance measures derived from dMRI and image analysis.

2) Deformities and abnormal dynamics of the thorax and abdomen in TIS present both before and after surgical intervention are precisely quantified for the first time, providing new scientific understanding of the biomechanical bases for TIS, and new objective measures of treatment response in TIS.

2. MATERIALS AND METHODS

The proposed methodology involves the following steps: (1) gathering image data; (2) 4D image construction; (3) 4D segmentation of lungs; and (4) defining landmarks and performing dynamic distance analysis.

2.1 Gathering image data

This retrospective study was conducted following approval from the Institutional Review Board at the Children's Hospital of Philadelphia along with a Health Insurance Portability and Accountability Act waiver. The data sets consist of 25 dynamic thoracic MRI scans from 25 TIS patients (age 3-10 years), both pre-operatively and roughly 1 year post-operatively, with voxel size ranging from $2.21\times2.21\times4.8$ mm^3 to $1.17\times1.17\times5.0$ mm^3 and 3D scene size varying from $192\times192\times31$ to $224\times256\times34$. MRI scan parameters using TrueFISP imaging sequences: TR/TE ~ 4.3/2.2 msec, magnetic field strength of 1.5 T. In our set up, for each sagittal slice position, slice images are acquired at a rate of about 200 ms/slice over several natural breathing cycles.

2.2 4D image construction

In our set up, for each of 35-45 sagittal slice (z-) positions, 80-100 slice MR images are acquired at ~ 200ms/slice over several tidal breathing cycles. This produces 2800-4500 slices per patient, which represent a digitization of the 4D free-breathing patient thorax over multiple breathing cycles. From this collection of slices, we need to extract one consistent 4D volume that represents the dynamic thorax over one respiratory cycle. We take a graph-based combinatorial optimization approach [5] for constructing the best possible 4D volume from such data entirely in the digital domain. This method guarantees a globally optimal solution. The constructed 4D image typically contains about 200-250 slices.

2.3 4D segmentation of structures

Before carrying out segmentation, the 4D images are processed to improve signal quality and consistency [6-8]. We first perform interactive non-uniformity correction and then intensity standardization as preprocessing steps. The dMRI

images have poor definition of the lung boundary due to low MRI signal from bone and other connective tissues in the vicinity of the lung boundary. We developed an interactive version of the Iterative Relative Fuzzy Connectedness method [9] wherein seeds are specified on slices in the lung tissue and in neighboring background tissues and segmentation is carried out in a slice by slice manner. Typically, the seeds can be propagated in adjoining slices without having to change them. The segmentation process proceeds under user supervision and when it goes wrong, the user intervenes and re-specifies seeds. Left and right lungs are segmented as separate objects.

2.4 Selecting landmark points and dynamic distance analysis

From the segmented lungs, we create a shape sketch to codify and then quantify the overall architecture of the key 4D dynamic thoraco-abdominal structure as follows. On the 3D object boundaries corresponding to each time point, we select a total of 18 key landmark points. With about 4 respiratory time points in each 4D volume, we have a total of 72 points which represent this dynamic architecture. Points are identified manually on the boundaries of the lungs and kidneys in sagittal sections, on segmented binary images for lungs and dMRI images for kidneys. For each lung, points are defined on three sagittal sections corresponding to locations that are most lateral (*L*), most medial (*M*), and at locations through the middle of the lung. For kidneys, the section selected is through the middle of each kidney which passes through the apex of the kidney. We use the following notation for denoting points as variables: *P-O-X-t*. *P* denotes that the variable is a point (*P*). *O* denotes the objects: *RL*(right lung), *LL*(left lung), *RK*(right kidney), and *LK*(left kidney). *X* denotes one of the 8 locations (see Figure 1 and Table 1): *L*, *M*, and superior (*S*), inferior (*I*), anterior (*A*), posterior (*P*), inferior-anterior (*IA*), and inferior-posterior (*IP*) at the middle of the lung. The following 4 time points over the full respiratory cycle from end-expiration to the next end-expiration are considered: end-expiration (*EE*), mid-inspiration (*MI*), end-inspiration (*EI*), and mid-expiration (*ME*).

We obtain a total of 144 landmark points for each subject (or patient) in both pre-operative and post-operative states. A detailed analysis is then carried out based on the 3D Euclidean distance measures denoted by d_1, d_2 ,…., d_{10}, as shown in Table 2 for specific anatomic distances. Since a significant number of our TIS patients have abnormal renal mobility, the 3D excursion of the kidneys (captured in d_2, d_5, d_7, d_8, and d_{10}) with respiration will gauge their contribution to obstruction of motion of the diaphragm. The above-mentioned distances quantify the overall displacements of key aspects of dynamic architecture, as shown in Figure 2.

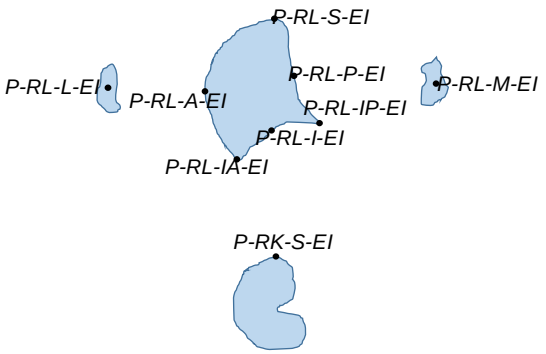

Figure 1. Schematic diagram of definition of landmark points on three sagittal sections of right lung (going from lateral to medial) and middle section of right kidney during end-inspiration.

We performed two types of analysis. For the first analysis task (see Table 3), we estimate the changes in distance relative to spinal curves. For the second analysis task (see Table 4), we estimate the changes from pre-operative to post-operative states through analyzing distances. Subscripts *Pr* and *Pt* in Table 4 represent pre- and post-operative states, respectively.

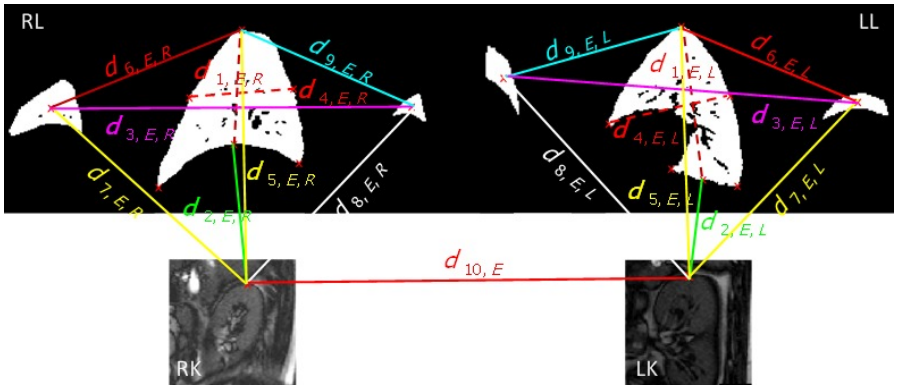

Figure 2. Distance definitions based on the obtained landmark points. Note that we utilize the segmented binary images for lungs and dMRI images for kidneys. The subscript *E* represents end-expiration, *R* right side, and *L* left side.

Table 1. Definition of landmark points to select		
Object (*O*)	Location (*X*)	Time point (*t*)
RL	*L, S, I, A, P, IA, IP, M*	*EE, MI, EI, ME*
LL	*L, S, I, A, P, IA, IP, M*	*EE, MI, EI, ME*
RK	*S* (*Apex of the kidney*)	*EE, MI, EI, ME*
LK	*S* (*Apex of the kidney*)	*EE, MI, EI, ME*

Table 2. Definition of 3D distances					
Distance	d_1	d_2	d_3	d_4	d_5
Description	*S* to *I*	*I* to *Apex*	*L* to *M*	*A* to *P*	*S* to *Apex*
Distance	d_6	d_7	d_8	d_9	d_{10}
Description	*S* to *L*	*L* to *Apex*	*Apex* to *M*	*M* to *S*	*Apex* to *Apex*

Table 3. Aim 1: To estimate the changes in distance relative to spinal curves (46 pairs)	
Comparison Pairs	Description
$d_{1,I,L}$ to $d_{1,E,L}$,…, $d_{9,I,L}$ to $d_{9,E,L}$	Compare *EI* with *EE* based on 9 distances of *LL*
$d_{1,I,R}$ to $d_{1,E,R}$,…, $d_{9,I,R}$ to $d_{9,E,R}$	Compare *EI* with *EE* based on 9 distances of *RL*
$d_{1,I,L}$ to $d_{1,I,R}$,…, $d_{9,I,L}$ to $d_{9,I,R}$	Compare *LL* with *RL* based on 9 distances in *EI*
$d_{1,E,L}$ to $d_{1,E,R}$,…, $d_{9,E,L}$ to $d_{9,E,R}$	Compare *LL* with *RL* based on 9 distances in *EE*
$(d_{1,I,L} - d_{1,E,L})$ to $(d_{1,I,R} - d_{1,E,R})$,.., $(d_{9,I,L} - d_{9,E,L})$ to $(d_{9,I,R} - d_{9,E,R})$	Compare differences of *LL* between *EI* and *EE* with differences of *RL* based on 9 distances
$d_{10,I}$ to $d_{10,E}$	Compare *EI* with *EE* based on the distance between *RK* and *LK*

Table 4. Aim 2: To estimate the improvements from pre- to post-operative states through analyzing distances	
Comparison Pairs	Description
$d_{1,I,L,Pr}$ to $d_{1,I,L,Pt}$,…, $d_{9,I,L,Pr}$ to $d_{9,I,L,Pt}$	Compare 9 distances in *EI* of *LL* in *Pr* with the distances in *Pt*
$d_{1,E,L,Pr}$ to $d_{1,E,L,Pt}$,…, $d_{9,E,L,Pr}$ to $d_{9,E,L,Pt}$	Compare 9 distances in *EE* of *LL* in *Pr* with the distances in *Pt*
$d_{1,I,R,Pr}$ to $d_{1,I,R,Pt}$,…, $d_{9,I,R,Pr}$ to $d_{9,I,R,Pt}$	Compare 9 distances in *EI* of *RL* in *Pr* with the distances in *Pt*
$d_{1,E,R,Pr}$ to $d_{1,E,R,Pt}$,…, $d_{9,E,R,Pr}$ to $d_{9,E,R,Pt}$	Compare 9 distances in *EE* of *RL* in *Pr* with the distances in *Pt*
$(d_{1,I,L,Pr} - d_{1,E,L,Pr})$ to $(d_{1,I,L,Pt} - d_{1,E,L,Pt})$,…, $(d_{9,I,L,Pr} - d_{9,E,L,Pr})$ to $(d_{9,I,L,Pt} - d_{9,E,L,Pt})$	Compare 9 distance differences of *LL* between *EI* and *EE* in *Pr* state with distance differences in *Pt* state
$(d_{1,I,R,Pr} - d_{1,E,R,Pr})$ to $(d_{1,I,R,Pt} - d_{1,E,R,Pt})$,…, $(d_{9,I,R,Pr} - d_{9,E,R,Pr})$ to $(d_{9,I,R,Pt} - d_{9,E,R,Pt})$	Compare 9 distance differences of *RL* between *EI* and *EE* in *Pr* state with distance differences in *Pt* state
$d_{10,I,Pr}$ to $d_{10,I,Pt}$	Compare distance between *RK* and *LK* in *EI* in *Pr* with distance in *Pt*
$d_{10,E,Pr}$ to $d_{10,E,Pt}$	Compare distance between *RK* and *LK* in *EE* in *Pr* with distance in *Pt*
$(d_{10,I,Pr} - d_{10,E,Pr})$ to $(d_{10,I,Pt} - d_{10,E,Pt})$	Compare difference between *EI* and *EE* in *Pr* state with difference in *Pt* based on distance between *RK* and *LK*

3. RESULTS

In all the comparison experiments performed in this study, paired *t*-test was conducted to assess whether the difference in 3D distance or distance difference between two matched samples was statistically significantly different, with a significance level set at $p< 0.05$. The null hypothesis *h* is that no difference exists between two matched samples in mean values of the evaluation metric. The *t*-statistic, which follows a *t*-distribution under the null hypothesis, is used as the test statistic to calculate the *p*-value and to decide whether to reject the null hypothesis.

3.1 Distance difference between left & right sides, end-inspiration & end-expiration

Table 5 lists the significant differences found between two matched 3D distances or distance differences. It contains a wealth of information about the dynamic thoraco-abdominal changes during respiration. For illustration, we consider five examples. (1) $d_{3,i,l} > d_{3,i,r}$: Medial to lateral distance in left lung in end-inspiration is greater than the same distance in right lung by over 16 mm on average. (2) $d_{7,i,l} < d_{7,i,r}$: Distance in end-inspiration from the apex of left kidney to the lateral point of left lung (*P-LL-L-EI*) is smaller than the corresponding distance on the right side by about 8 mm.(3) $d_{2,e,l} < d_{2,e,r}$: Distance in end-expiration from the base of *LL* to the apex of left kidney (*LK*) is smaller than the corresponding distance on the right by about 10 mm. (4) $d_{9,e,l} < d_{9,e,r}$: Apex to the medial distance in end-expiration of *LL* is smaller than the distance of *RL* by about 18 mm. (5) $d_{1,i,l} - d_{1,e,l} < d_{1,i,r} - d_{1,e,r}$: Apex to the base distance difference of *LL* between end-inspiration and end-expiration is smaller than the distance difference of *RL* with the difference of mean distance difference by about 2 mm. Most of the significant differences found as listed in Table 5 are between the left and the right side.

Table 5. Significant differences between two matched samples performed by paired *t*-test for Aim 1

Comparison Pair	*p*	*mean* (*sd*) (mm)
$d_{2,i,r}$ to $d_{2,e,r}$	0.0061	-1.74 (4.24)
$d_{5,i,r}$ to $d_{5,e,r}$	0.0085	1.5 (3.82)
$d_{2,i,l}$ to $d_{2,i,r}$	0.0279	-9.41 (26)
$d_{3,i,l}$ to $d_{3,i,r}$	0.0006	15.51 (29.74)
$d_{4,i,l}$ to $d_{4,i,r}$	0.0306	-7.23 (22.93)
$d_{7,i,l}$ to $d_{7,i,r}$	0.0126	-7.83 (17.42)
$d_{9,i,l}$ to $d_{9,i,r}$	0.0051	-19.99 (48.17)
$d_{2,e,l}$ to $d_{2,e,r}$	0.0163	-9.99 (26.53)
$d_{3,e,l}$ to $d_{3,e,r}$	0.00004	17.76(27.75)
$d_{7,e,l}$ to $d_{7,e,r}$	0.0036	-9.98 (19.55)
$d_{9,e,l}$ to $d_{9,e,r}$	0.0092	-18.11 (47.2)
$(d_{1,i,l} - d_{1,e,l})$ to $(d_{1,i,r} - d_{1,e,r})$	0.0161	-2.37 (6.71)

Table 6. Significant differences between two matched samples performed by paired *t*-test for Aim 2

Comparison Pair	*p*	*mean* (*sd*) (mm)
$d_{1,i,r,pr}$ to $d_{1,i,r,po}$	0.0061	-8.89 (16.89)
$d_{6,i,r,pr}$ to $d_{6,i,r,po}$	0.0085	-10.17 (18.6)
$d_{6,e,r,pr}$ to $d_{6,e,r,po}$	0.0279	-10.57 (17.05)
$(d_{1,i,l,pr} - d_{1,e,l,pr})$ to $(d_{1,i,l,po} - d_{1,e,l,po})$	0.0006	-3.68 (7.82)
$(d_{4,i,r,pr} - d_{4,e,r,pr})$ to $(d_{4,i,r,po} - d_{4,e,r,po})$	0.0306	3.82 (7.81)

3.2 Distance change from pre- to post-operative state

As shown in Table 6, following surgery, our analysis shows, on average, an 8.89 mm (7.7%) increase in superior to inferior distance of the right lung in end-inspiration, a 10.17 mm (9.4%) increase in superior to lateral distance of right lung in end-inspiration, a 10.57 mm (10.6%) increase in superior to lateral distance of the right lung in end-expiration, and a 3.82 mm (86.7%) reduction in anterior to posterior distance difference of the right lung between end-inspiration

and end-expiration. These results suggest reversal of the abnormalities associated with TIS following surgical intervention.

4. CONCLUSIONS

This paper introduces a novel approach to construct a quantitative biomechanical understanding of the thorax and upper abdomen from dynamic MRI in patients with TIS, and to develop new thoraco-abdominal dynamic organ architectural quantitative measures derived from dMRI. In particular, a shape sketch is created to codify and then quantify the overall architecture, which involves the selection of 3D landmark points and computation of 3D dynamic distances over a full respiratory cycle. We perform two statistical analyses of distance sketches on 25 TIS patients to try to understand the pathophysiological mechanisms in TIS and to quantitatively evaluate improvements from pre-operative to post-operative states. Further exploration of dynamic thoraco-abdominal architecture and relation to surgical treatment and clinical parameters is ongoing.

Acknowledgements

This research was supported by a grant from the National Institutes of Health 1R21HL124462-01A1 and a "Frontier" grant from the Children's Hospital of Philadelphia. The visit of Mr. Jie Song to the Medical Image Processing Group for one year was supported by the China Scholarship Council (CSC) Grant #201606840085.

REFERENCES

[1] Campbell R M, smith M D. "Thoracic insufficiency syndrome and exotic scoliosis," J Bone Surg Am. 89 Suppl 1:108-22 (2007).

[2] Mayer O. H., Redding G., "Change in Cobb angle and lung function after VEPTR insertion in children with thoracic insufficiency syndrome," Am. J. Respir. Crit. Care Med., 175:A721 (2007).

[3] Redding G., Song K., Inscore S. et. al., "Lung function asymmetry in children with congenital and infantile scoliosis," Spine, vol. 8, no. 4, 639–644 (2007).

[4] Tong Y, Udupa J. K., Wileyto E.P., Wu C., McDonough J.M., Capraro A., Torigian D.A., Campbell R.M. Quantitative dynamic MRI (QdMRI) Volumetric Analysis of Pediatric Patients with Thoracic Insufficiency Syndrome, Proceedings of SPIE Medical Imaging Conference, 2018, to appear.

[5] Tong Y, Udupa J. K., Ciesielski K. C., McDonough J. M., Mong A, Campbell R. M., "Retrospective 4D MR image construction from free-breathing slice Acquisitions: A novel graph-based approach" Medical Image Analysis, vol. 35, 345-359 (2017).

[6] Tustison N. J., Avants B. B., Cook P. A., Zheng Y., Egan A., Yushkevich P. A., Gee J. C.. "N4ITK: improved N3 bias correction," IEEE Trans. Med. Imaging, vol. 29, no. 6, 1310-1320 (2010).

[7] Madabhushi A., Udupa J.K., "Interplay between intensity standardization and inhomogeneity correction in MR image processing," IEEE Trans. Med. Imaging, vol. 24, no. 5, 561-576(2005).

[8] Tong Y., Udupa J. K., Odhner D., Sharma S., Torigian D. A.,"Interactive non-uniformity correction and intensity standardization of MR images," Conf Proc SPIE. 9415, 94151N-1 - 94151N-6 (2015).

[9] Tong Y., Udupa J. K., Odhner D., Wu C., Zhao Y., McDonough J. M., Capraro A., Torigian D. A., Campbell R. M., "Interactive iterative relative fuzzy connectedness lung segmentation on thoracic 4D dynamic MR images," SPIE Proceedings of Medical Imaging Conference. 10137, 1-6 (2017).